

All-optical logic gate based on manipulation of surface polaritons solitons via external gradient magnetic fields

Qi Liu, Na Li, and Chaohua Tan ^{*}

School of Physics and Electronics, Shandong Normal University, Jinan 250014, China

 (Received 10 September 2019; accepted 24 January 2020; published 12 February 2020)

We theoretically study the magneto-optical manipulation of surface polaritons (SPs) in the negative index metamaterial–dielectric interface waveguide system. We analyze the linear and nonlinear propagation properties of the system when a weak gradient magnetic field is applied. A lossless superluminal SPs soliton is obtained via active Raman gain. We show that the SPs soliton will deflect in the weak gradient magnetic field (Stern-Gerlach-like effect); thus, the trajectory of SPs can be controlled by the gradient magnetic field, and dynamic control of SPs can also be realized by using a time-dependent gradient magnetic field. In addition, a “XNOR”-like logic gate is realized based on the trajectory control of SPs with external magnetic field and the interaction of the SPs soliton. This paper has certain theoretical significance for nanoscale optical information processing.

DOI: [10.1103/PhysRevA.101.023818](https://doi.org/10.1103/PhysRevA.101.023818)

I. INTRODUCTION

The surface-plasmon polariton (SPP) is a strongly confined electromagnetic (EM) mode associated with collective surface-plasmon oscillation. It confines the EM energy into the subwavelength space region near the metal-dielectric interface, which makes it promising for future on chips integrated optics [1], quantum plasmonic circuitry [2], etc. Thus, SPPs have huge potential for nanoscale quantum information processing and communication.

However, the practical application of SPPs is limited by the high Ohmic loss in metals. Several schemes for compensating the Ohmic loss have been proposed. In 2008, Kamli *et al.* suggested to replace the metal with negative-index metamaterial (NIMM) and place an electromagnetically induced transparency medium at the NIMM-dielectric interface [3]. They found that the surface polaritons (SPs), the surface electromagnetic waves propagating along a dielectric-NIMM interface, can propagate with very small attenuation. Then, this technic was developed to obtain large phase shifts [4], maximum entangled states of two optical pulses [5], and slow light propagation [6] of SPs, while simultaneously avoiding losses. More recently, the lossless SPs scheme was extended for nonlinear-SPs rogue waves and breathers excitation, and frequency-comb generation [7,8]. Gain-assisted schemes can also compensate Ohmic loss, such as electromagnetically induced gain [9]. Furthermore, other gain schemes including coherent population oscillation [10] and active Raman gain (ARG) [11] have been used in the NIMM-dielectric interface to excite low-loss nonlinear-SPs solitons.

On the road towards practical SPP and SPs devices, not only Ohmic loss needs to be overcome, but also the effective manipulating methods need to be explored. Such methods have been widely studied, such as nanostructure engineering

[12,13] and active plasmonic technologies [1,14–16]. And to active control SPPs and SPs, external field is needed. Recently, many researchers have shown special interest in controlling SPPs with external magnetic field and have made great progresses, such as transmission control [17,18], intense modulation [19], ultrafast switches [20], etc.

Nevertheless, the track manipulation of SPPs with external magnetic field may be attractive for designing novel optical integrated circuits components. Manipulation of laser beams via external gradient magnetic fields in atomic gases has been observed and studied extensively, which is known as the optical Stern-Gerlach effect [21–25]. But to our knowledge, such effect has not yet been reported on SPPs or SPs.

In this paper, we propose a scheme to manipulate SPs via external magnetic field in the NIMM-dielectric interface waveguide, and achieve the ultra-low-loss propagation of SPs solitons via ARG. We show that the propagation track of SPs solitons is controllable as the form of the gradient function of external static magnetic field changes, and a dynamic manipulation is realized when a time-dependent gradient magnetic field is applied. Furthermore, an all-optical “XNOR”-like logic gate is demonstrated based on a specially designed gradient magnetic field and the SPs soliton interaction.

II. THEORETICAL MODEL

We consider a planar waveguide system consisting of a NIMM and dielectric. We assume the NIMM occupies the lower half-infinity plane while the dielectric stays in the upper half-infinity plane as shown in Fig. 1(a). ϵ_1 (ϵ_2) and μ_1 (μ_2) is permittivity and permeability of the NIMM (dielectric), respectively, and the frequency dependencies of ϵ_1 and μ_1 are given by the Drude model [3] in the optical region. The dielectric is chosen as the ARG medium, which has a Λ -type energy-levels configuration [Fig. 1(b)], interacting with a weak, pulsed probe field at center angular frequency ω_p (coupling with $|2\rangle \leftrightarrow |3\rangle$ transition) and a strong,

^{*}tanch@sdnu.edu.cn

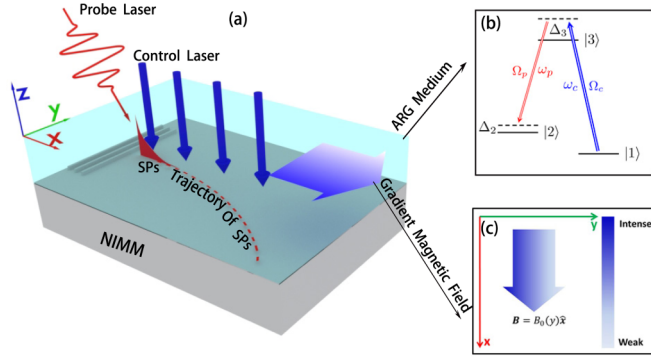


FIG. 1. (a) A schematic of manipulating ultra-low-loss SPs in a NIMM dielectric interface waveguide. The waveguide is structured by a half-space NIMM and half-space ARG medium. The SPs wave is excited by an obliquely incident probe laser, and the vertically incident control laser provides an active gain to balance absorption. (b) Δ -type energy configuration of the ARG medium. To obtain a suitable gain and suppress the Doppler effect, the control field is far detuned by Δ_3 . (c) Applied magnetic field to manipulate the SPs. The magnetic field is along the waveguide interface in the x direction and the gradient direction is parallel to the y axis.

continuous-wave control field at center angular frequency ω_c with a far detuning (coupling with $|1\rangle \leftrightarrow |3\rangle$ transition). The probe field is chosen as the transverse magnetic (TM) mode of SPs, and the control field is chosen as the plane wave. There exist decay phenomena due to the finite lifetime of state $|j\rangle$, which is described by decay rate γ_j ($j = 2, 3$). Two-photon (one-photon) detuning is represented by Δ_2 (Δ_3). Note that the decay γ_j is introduced phenomenologically to describe the dephasing of the system, which is mainly contributed by spontaneous emission, and also includes other dephasing processes, such as elastic collision. The coordinate system is set as illustrated in Fig. 1(a). The SPs are excited and propagate along the interface of the waveguide in the x direction while the control field is vertically incident. The corresponding electric field of the probe and control field are $\mathbf{E}_p = \mathcal{E}_p(x, y, t)\mathbf{u}_p(z)\exp[i(\beta x - \omega_p t)] + \text{c.c.}$ and $\mathbf{E}_c = \mathcal{E}_c\hat{\mathbf{y}}\exp[i(k_c z - \omega_c t)] + \text{c.c.}$, where \mathcal{E}_l ($l = p, c$) is the amplitude of the electric field, $\mathbf{u}_p(z)$ is the mode function in the z direction resulting from the dielectric-NIMM interface, and $\beta(\omega_p) = \omega_p[\epsilon_{r1}\epsilon_{r2}(\epsilon_{r1}\mu_{r2} - \epsilon_{r2}\mu_{r1})/(\epsilon_{r1}^2 - \epsilon_{r2}^2)]^{1/2}/c$ and k_c are the propagate constant of the probe field and control field, respectively. The imaginary part of the $\beta(\omega_p)$ characterizes the absorption of the waveguide, which is contributed by both electric and magnetic absorption response of the NIMM. The optical frequency ω_p is chosen to make the electric and magnetic absorption destructive interference, thus the total absorption is largely reduced [3, 8, 10]. The explicit expressions of the EM field are given in Appendix A.

An external gradient magnetic field is parallel to the x direction and inhomogeneous in the y direction [Fig. 1(c)]; such magnetic field is described by $\mathbf{B}(y) = B_0(y)\hat{\mathbf{x}}$. The existence of the external magnetic field will cause a Zeeman level shift of energy level E_j , which reads $\Delta E_{j,\text{Zeeman}} = \mu_B g_F^j m_F^j B_0(y)$ with μ_B the Bohr magneton, g_F^j the gyromagnetic factor, m_F^j the magnetic quantum number, and superscript j indicating the state number. The energy shift finally induces a correction

to the detuning: $\Delta'_{2(3)} = \Delta_{2(3)} - \mu_{2(3)1} B_0(y)$, where $\mu_{jl} = \mu_B(g_F^j m_F^j - g_F^l m_F^l)/\hbar$. Here, \hbar is Planck's constant.

In the interaction picture with electric dipole and rotating-wave approximations, the Hamiltonian of the system reads $\hat{H}_I = -\hbar \sum_j \Delta'_j |j\rangle\langle j| - \hbar[\Omega_c |3\rangle\langle 1| + \exp(i\theta_p) \zeta_p(z)\Omega_p |3\rangle\langle 2| + \text{H.c.}]$, where $\Omega_c = (\hat{\mathbf{y}} \cdot \mathbf{p}_{13})\mathcal{E}_c/\hbar$, $\Omega_p = |\mathbf{p}_{23}|\mathcal{E}_p(x, y, t)/\hbar$, $\zeta_p(z) = \mathbf{u}_p(z) \cdot \mathbf{e}_{23}$. Here, \mathbf{p}_{jl} is the electric dipole matrix element related to the states $|j\rangle$ and $|l\rangle$, and $\theta_p = [\beta + k_2 - k_3]x$ is the phase mismatch caused by the eigendispersion β of SPs, with $k_{2(3)}$ the wave number of state $|2(3)\rangle$.

Deriving from the Schrödinger equation and Maxwell equation, we can obtain the dynamic equations of the system, which read

$$\left(i\frac{\partial}{\partial t} + d_2\right)A_2 + e^{-i\theta_p}\zeta_p^*(z)\Omega_p^*A_3 = 0, \quad (1a)$$

$$\left(i\frac{\partial}{\partial t} + d_3\right)A_3 + e^{i\theta_p}\zeta_p(z)\Omega_p A_2 + \Omega_c A_1 = 0, \quad (1b)$$

$$|A_1|^2 + |A_2|^2 + |A_3|^2 = 1, \quad (1c)$$

$$e^{i\theta_p}\zeta_p(z)\left(\hat{L} + \frac{1}{2\beta}\frac{\partial^2}{\partial y^2}\right)\Omega_p + \kappa_{23}A_3A_2^* = 0, \quad (1d)$$

$$\hat{L} = i\left(\frac{\partial}{\partial x} + \frac{1}{n_{\text{eff}}}\frac{1}{c}\frac{\partial}{\partial t}\right), \quad (1e)$$

with A_j the state amplitude of state $|j\rangle$; $d_{2(3)} = \Delta'_{2(3)} + i\gamma_{2(3)}$ the dephasing parameter; \hat{L} the wave operator; n_{eff} and c the effective refractive index and speed of light in vacuum, respectively; and $\kappa_{23} = \mathcal{N}_a |\mathbf{p}_{23}|^2 \omega_p^2 / (2\epsilon_0 \hbar \beta c^2)$ the coupling strength where \mathcal{N}_a is atoms concentration and ϵ_0 is permittivity of free space. Note that our system is under the ARG scheme, which is off-resonant excitation; thus, using the amplitude equations based on the Schrödinger equation together with the Maxwell equation is still a good approach to describe the system [26].

Based on the multiscale method [26], the asymptotic expansions are used: $A_j = A_j^{(0)} + \epsilon^1 A_j^{(1)} + \epsilon^2 A_j^{(2)} + \dots$, ($j = 1, 2, 3$), $d_j = d_j^{(0)} + \epsilon^1 d_j^{(1)} + \epsilon^2 d_j^{(2)}$, ($j = 2, 3$), $\Omega_p = \epsilon^1 \Omega_p^{(1)} + \epsilon^2 \Omega_p^{(2)} + \dots$. To obtain a divergence-free expansion, all quantities on the right-hand side of the expansions are considered as functions of the multiscale variables $z_l = \epsilon^l z$ ($l = 0, 1, 2$) and $t_l = \epsilon^l t$ ($l = 0, 1$). Here, ϵ is a dimensionless small parameter characterizing the typical amplitude ratio of the probe field and the control field. Then Eqs. (1a)–(1d) can be solved order by order.

III. THE LINEAR PROPERTY OF THE SYSTEM

First, we will show the possibility to make ultra-low-loss propagating SPs via ARG. To this end, we analyze the linear dispersion property of the system. When the probe field is absent (corresponding to the zeroth-order solution), the state amplitude of the system reads $A_1^{(0)} = |d_3^{(0)}|/\sqrt{|\Omega_c|^2 + |d_3^{(0)}|^2}$, $A_2^{(0)} = 0$, and $A_3^{(0)} = -\Omega_c A_1^{(0)}/d_3^{(0)}$ with $d_{2(3)}^{(0)} = \Delta_{2(3)} + i\gamma_{2(3)}$. Due to the fact that the control laser is vertically incident, the steady state is homogeneous.

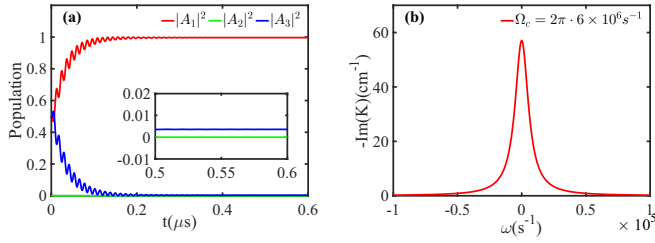


FIG. 2. (a) Time evolution of the population in states $|1\rangle$ (red line), $|2\rangle$ (green line), and $|3\rangle$ (blue line). (b) Negative imaginary part (gain) $-\text{Im}(K)$ as a function of ω .

Notice that the external magnetic field is assumed to be the order of ϵ^2 ; thus, it has no effect on the zeroth-order solution, or on the first-order solution, i.e., the linear dispersion property. The first-order solution is $\Omega_p^{(1)} = \mathcal{F}e^{i\theta}$ with $\theta = (K(\omega)x_0 - \omega t_0)$ and \mathcal{F} is a slowly varying envelope function of multiscale variables yet to be determined. Following the calculated routine we obtain the linear dispersion of SPs interacting with the ARG medium:

$$K(\omega) = \frac{1}{n_{\text{eff}}} \frac{\omega}{c} + \kappa_{23} \frac{|A_3^{(0)}|^2}{\omega - d_2^{*(0)}}. \quad (2)$$

The explicit expressions of the first-order solution are given in Appendix B. We should be aware that ω is the angular frequency shift to the center frequency ω_p . The imaginary part of $K(\omega)$ characterizes the linear absorption (positive sign) or gain (negative sign) of the probe field, which reads

$$\tilde{K}(\omega) = -\frac{\kappa_{23}\gamma_2|A_3^{(0)}|^2}{(\omega - \Delta_2)^2 + \gamma_2^2}. \quad (3)$$

Figure 2(a) shows the time evolution of the population in states $|1\rangle$ (red line), $|2\rangle$ (green line), and $|3\rangle$ (blue line). System parameters of the ARG medium are chosen as $\gamma_1 = 0$, $\gamma_2 = 2\pi \times 10^3 \text{ s}^{-1}$, $\gamma_3 = 2\pi \times 3 \times 10^6 \text{ s}^{-1}$ [27,28]. Other parameters are $\Delta_2 = 0$, $\Delta_3 = 2\pi \times 10^8 \text{ s}^{-1}$, $\Omega_c = 2\pi \times 6 \times 10^6 \text{ s}^{-1}$. In Fig. 2(a), the initial-states amplitude is $A_1 = A_3 = 1/\sqrt{2}$, $A_2 = 0$, and the probe field is absent ($\Omega_p = 0$); we can find that the population on state $|3\rangle$ is oscillating, and damping quickly, and becoming stable, and the nonvanishing population on state $|3\rangle$ can provide an active gain to the SPs.

In Eq. (3), we know that, as long as the population on state $|3\rangle$ is not vanished (i.e., $A_3^{(0)} \neq 0$) or, equivalently, the strong control field is present in the system, the sign on the right-hand side of Eq. (3) keeps negative, which means the probe SPs always receive a gain from the system. Shown in Fig. 2(b) is the gain spectrum $-\text{Im}[K(\omega)]$ [with $\kappa_{23} = 1 \times 10^8 \text{ cm}^{-1} \text{ s}^{-1}$; other parameters are the same as those in Fig. 2(a)], which is resulted from the nonvanished population on state $|3\rangle$.

According to the previous work [3,10], in order to reserve the longitudinal compression of the SPs, the center frequency ω_p is located in the domain where there exists absorption (caused by Ohmic loss), i.e., $\tilde{\beta}(\omega_p) = \text{Im}[\beta(\omega_p)] > 0$. When the eigenabsorption caused by Ohmic loss and linear gain provided by the ARG medium is balanced, the SPs will propagate without any loss. Then we get the no loss condition: $\tilde{K}(\omega) + \tilde{\beta}(\omega_p) = 0$. This condition indicates that we can

adjust the two-photon detuning Δ_2 to obtain lossless SPs, and the special detuning reads

$$\Delta_{2,\text{lossless}} = \omega \pm \frac{\sqrt{\gamma_2 \tilde{\beta}(\omega_p) [\kappa_{23} |A_3^{(0)}|^2 - \gamma_2 \tilde{\beta}(\omega_p)]}}{\tilde{\beta}(\omega_p)}. \quad (4)$$

In a realistic system, when the detuning Δ_2 is near the value as in Eq. (4), the lossless condition is still satisfied approximately. In other words, an ultra-low-loss SP is possible to obtain in this system.

Further more, it can be seen from the above analysis that whether the control field is on or off is essential. If we turn off the control field, the linear gain will disappear and the SPs suffer from a severe eigenabsorption. Such a controllable absorption of the SPs scheme is useful to design modulators or all-optical switches [1,16].

IV. MANIPULATING THE SP SOLITON VIA THE GRADIENT MAGNETIC FIELD

The first-order solution gives the linear dispersion of the SPs, as well as all high-order dispersion relations: $K_l(\omega) = \partial^l K(\omega) / \partial \omega^l$ ($l = 1, 2, 3, \dots$). Nevertheless, we are more interested in a shape-preserving propagation of the probe field, i.e., the SPs soliton. Thus we will derive the nonlinear evolution equation of the probe field.

In the second order, a divergency-free solution of $\Omega_p^{(2)}$ requires

$$\frac{\partial \mathcal{F}}{\partial x_1} + \frac{1}{V_g} \frac{\partial \mathcal{F}}{\partial t_1} = 0, \quad (5)$$

which means the envelope \mathcal{F} travels with complex group velocity $V_g = K_1^{-1}$. In this system, due to the ARG effect, the group velocity of the SPs can be superluminal, i.e., the group velocity $v_g = \text{Re}[V_g] < 0$ [29,30]. Another favorable feature of our system is the giant Kerr effect. On the one hand, the ARG medium provides a considerable nonlinearity which is approximately 10^{11} times larger than the conventional one [31]. On the other hand, the waveguide system tightly confines the EM field to the interface, and the light-matter interaction is enhanced locally, which produces an extra enhancement on nonlinearity. Thus, in such a lossless system, it is easy to balance the dispersion (or diffraction) and the nonlinearity, and to obtain SPs solitons.

In the third-order solutions, the solvability of third order $\Omega_p^{(3)}$ gives

$$i \left(\frac{\partial \mathcal{F}}{\partial x_2} + \frac{1}{V_g} \frac{\partial \mathcal{F}}{\partial t_2} \right) + \frac{1}{2\beta} \frac{\partial^2 \mathcal{F}}{\partial y_1^2} - \frac{K_2}{2} \frac{\partial^2 \mathcal{F}}{\partial t_1^2} + W |\mathcal{F}|^2 \mathcal{F} e^{-2\tilde{\alpha}x_2} + M B^{(2)} \mathcal{F} = 0, \quad (6)$$

with the average nonlinear coefficient

$$W = \frac{\kappa_{23}}{\omega - d_2^{*(0)}} (A_3^{*(0)} a_{31}^{(2)} + A_3^{(0)} a_{31}^{*(2)}) g_e \quad (7)$$

and

$$M = -\frac{\kappa_{23}}{\omega - d_2^{*(0)}} \left\{ \frac{|A_3^{(0)}|^2 \mu_{21}}{\omega - d_2^{*(0)}} - \left[\left(1 - \frac{\Delta_3 |A_3^{(0)}|^2}{d_3^{*(0)}} \right) \frac{|A_3^{(0)}|^2}{d_3^{(0)}} + \text{c.c.} \right] \mu_{31} \right\}, \quad (8)$$

and $B^{(2)} = B(y)/\epsilon^2$. Coefficient $a_{31}^{(2)}$ is given in Appendix B. Here, $g_e = \int |\zeta_p(z)|^4 dz / \int |\zeta_p(z)|^2 dz$ is the enhancement factor due to the waveguide confinement. Then the self-Kerr susceptibility reads

$$\chi^{(3)} = \frac{2c}{\omega_p} \frac{|\mathbf{p}_{23}|^2}{\hbar^2} W = g_e \chi_0^{(3)}, \quad (9)$$

where \mathbf{p}_{23} is the transition dipole matrix element corresponding to the probe transition, and $\chi_0^{(3)}$ is the Kerr susceptibility in the no-waveguide system [31].

Combining Eqs. (5) and (6), and returning to the original variables, we can obtain the evolution equation of envelope $U = \Omega_p \exp(-i\alpha x)$:

$$i \left(\frac{\partial}{\partial x} + \frac{1}{V_g} \frac{\partial}{\partial t} + \alpha \right) U + \frac{1}{2\beta} \frac{\partial^2 U}{\partial y^2} - \frac{K_2}{2} \frac{\partial^2 U}{\partial t^2} + W|U|^2 U + MB(y)U = 0, \quad (10)$$

with $\alpha = \text{Im}[\beta(\omega_p) + K(0)]$.

We make a Galileo transformation and normalize the variables to their typical scales, i.e., $u = U/U_0$, $s = (x - v_g t)/L_{\text{Diff}}$, $\xi = y/R_y$, $\tau = t/\tau_0$, with R_y the transverse radius of the probe pulse, $L_{\text{Diff}} = \beta R_y^2$ the typical diffraction length, U_0 the typical Rabi frequency, τ_0 the pulse duration of the probe pulse, and the bar over the symbol denoting its real part. Then we obtain the dimensionless form of Eq. (10):

$$\frac{i}{\lambda} \frac{\partial u}{\partial \tau} + \frac{1}{2} \frac{\partial^2 u}{\partial \xi^2} + g_1 |u|^2 u + g_2(\xi, \tau) u = -ig_3 u + \frac{g_4}{2} \left(\lambda^2 \frac{\partial^2 u}{\partial s^2} - 2\lambda \frac{\partial^2 u}{\partial \tau \partial s} + \frac{\partial^2 u}{\partial \tau^2} \right), \quad (11)$$

with $g_1 = L_{\text{Diff}}/L_N$, $g_2 = L_{\text{Diff}} MB(\xi, \tau)$, $g_3 = L_{\text{Diff}}/L_A$, $g_4 = L_{\text{Diff}}/L_{\text{Disp}}$, $\lambda = v_g \tau_0/L_{\text{Diff}}$. And $L_N = 1/U_0^2 \text{Re}(W)$, $L_A = 1/\alpha$, and $L_{\text{Disp}} = \tau_0^2/\text{Re}(K_2)$ are typical nonlinear length, absorption length, and group velocity dispersion length, respectively.

Considering a probe field with large pulse duration τ_0 , such that the group-velocity dispersion [GVD, $K_2(\omega)$] will not take effect over the finite ARG medium length, i.e., $g_4 \ll 1$, and using the method we discussed in the previous section, the absorption can be made negligibly small, then $g_3 \ll 1$. Thus Eq. (11) is simplified to

$$\frac{i}{\lambda} \frac{\partial u}{\partial \tau} + \frac{1}{2} \frac{\partial^2 u}{\partial \xi^2} + g_1 |u|^2 u + g_2(\xi, \tau) u = 0, \quad (12)$$

which is a nonlinear Schrödinger equation with an external potential $g_2(\xi, \tau)$ resulting from the external magnetic field. The terms proportional to λ and λ^2 are also neglected; we will show the reason later. Note that the imaginary parts of all coefficients in the equation are ignored. This is valid if a realistic set of parameters can be found to make the imaginary

part of these coefficients negligibly small compared with their corresponding real parts. When the nonlinearity balances the diffraction effect, $g_1 = 1$ and thus the typical Rabi frequency reads $U_0 = 1/\sqrt{\beta|\bar{W}|R_y^2}$.

It is obvious that variable s is not apparent in Eq. (12), thus we can write the solution of this equation as $u(\tau, s, \xi) = w(s)v(\tau, \xi)$, where $w(s)$ is a traveling wave function describing the propagation character along the x direction. After integrating over the variable s , Eq. (12) becomes

$$\frac{i}{\lambda} \frac{\partial v}{\partial \tau} + \frac{1}{2} \frac{\partial^2 v}{\partial \xi^2} + \bar{g}_1 |v|^2 v + g_2(\xi, \tau) v = 0, \quad (13)$$

with $\bar{g}_1 = g_1 \int_{-\infty}^{\infty} |w|^2 ds / \int_{-\infty}^{\infty} w ds$. Without loss of generality, we take it as a Gaussian profile $w(s) = (1/\sqrt{2\pi\rho_0^2}) \exp[-s^2/(2\rho_0^2)]$, and ρ_0 is a free parameter. This means the SPs soliton propagates with x component $x = v_g t = L_{\text{Diff}} \lambda \tau$. With the above assumption, the terms proportional to λ and λ^2 in Eq. (11) are vanished after integrating over s .

Following the equivalent-particle theory [32,33], we get the shape-preserving solution of Eq. (13):

$$v(\tau', \xi) = \eta \text{sech}\{\eta[\xi - \xi_p(\tau')]\} \exp\{i[v_p(\tau')\xi + \sigma(\tau')]\}, \quad (14)$$

where $\xi_p(\tau') = \langle \xi \rangle_T$ is the central position of the soliton, $v_p(\tau') = d\xi_p/d\tau'$, $d\sigma/d\tau' = [\eta^2 - v_p^2(\tau')]/2$ where η is the amplitude parameter, and $\tau' = \lambda\tau$. The operator $\langle f \rangle_T = \int_{-\infty}^{+\infty} f |v|^2 d\xi / \int_{-\infty}^{+\infty} |v|^2 d\xi$ donates the transverse average value. The solution reveals that the soliton will obtain a transverse velocity v_p , and then obtain a transverse position shift ξ_p . The equation of transverse motion reads [32,33]

$$\frac{d^2 \xi_p}{d\tau'^2} = -\frac{\partial U_p}{\partial \xi_p}, \quad (15)$$

with U_p the equivalent potential, $\partial_{\xi_p} U_p = -(\partial_{\xi} g_2)_T$, and the initial values are $\xi_p(0) = \xi_0$, $\xi_p'(0) = 0$. When the external magnetic field is absent ($g_2 = 0$) or homogeneous, $\xi_p = \xi_0$, $v_p = 0$, the SPs soliton will keep its propagate direction under this condition.

We choose a set of realistic parameters to perform our analysis. The corresponding energy levels of the ARG medium are $|1\rangle = |5^2 S_{1/2}, F = 2, m_F = 2\rangle$, $g_F = -1/3$, $|2\rangle = |5^2 S_{1/2}, F = 3, m_F = 2\rangle$, $g_F = 1/3$, $|3\rangle = |5^2 P_{3/2}, F = 3, m_F = 2\rangle$, $g_F = 7/18$ [28]. The decay rates parameters are the same as the former section; other parameters read $\tau_0 = 5 \mu\text{s}$, $\Delta_2 = 2\pi \times 1.4 \times 10^5 \text{ s}^{-1}$, $\Delta_3 = 2\pi \times 5.2 \times 10^8 \text{ s}^{-1}$, $\Omega_c = 2\pi \times 5 \times 10^7 \text{ s}^{-1}$, $\kappa_{23} = 1 \times 10^9 \text{ cm}^{-1} \text{ s}^{-1}$, $R_y = 10 \mu\text{m}$, $\omega_c \approx \omega_p = 2\pi \times 3.85 \times 10^{14} \text{ s}^{-1}$ (corresponds to wavelength $\lambda_c \approx \lambda_p = 780 \text{ nm}$), $\beta(\omega_p) = (9.19 + 0.00013) \times 10^4 \text{ cm}^{-1}$, then $U_0 = 2\pi \times 4.98 \times 10^6 \text{ s}^{-1}$, $K = (-1.03 + 0.0072i) \times 10 \text{ cm}^{-1}$, $K_1 = -(1.15 + 0.016) \times 10^{-1} \text{ s cm}^{-1}$, $K_2 = -(2.58 + 0.054) \times 10^{-11} \text{ s}^2 \text{ cm}^{-1}$, $W = (1.11 + 0.0078) \times 10^{-13} \text{ s}^2 \text{ cm}^{-1}$, $L_{\text{Diff}} = 0.92 \text{ mm}$, $L_{\text{disp}} = 9.71 \text{ mm}$, $L_{\text{abs}} = 1/\alpha = 7.91 \text{ mm}$, $\lambda \approx -5$, $M = -(1.35 + 0.019i) \times 10^8 \text{ m}^{-1} \text{ T}^{-1}$. It is obvious that the dispersion length and absorption length are much longer than diffraction length, thus it is reasonable to neglect the GVD term in Eq. (11). And for the coefficients in Eq. (12), the imaginary parts are indeed much smaller than their corresponding real parts, and, as a

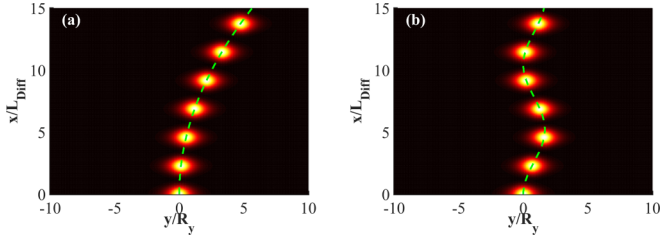


FIG. 3. Deflection of the SPs soliton. The bright light spots represent $|\Omega_p/U_0|$. Traveling trajectory of the SP soliton under the action of (a) linear gradient magnetic field $B_0(y) = k_L y$ (with gradient $k_L = -0.04 \text{ T m}^{-1}$) and (b) time-dependent linear gradient magnetic field $B_0(y, t) = k_T f(t) y$ [with $k_T = -0.3 \text{ T m}^{-1}$, $f(t) = \cos(3t/\tau_0)$]. The green dashed lines in panels (a) and (b) are theoretical trajectory calculated from Eq. (15).

result, to drop the imaginary part for these coefficients is also reliable.

Shown in Fig. 3 are the wave shape $|\Omega_p/U_0|$ for a single superluminal SPs soliton and its trajectory deflection under the external gradient magnetic field, which is obtained numerically from Eq. (12).

Figure 3(a) shows the deflect effect of the SPs soliton with a static external magnetic field $B_0(y) = k_L y$ with gradient $k_L = -0.04 \text{ T m}^{-1}$. In this case, the equivalent potential $U_p = -k_L \mathcal{M} \xi_p$, with $\mathcal{M} = \bar{M} \bar{\beta} R_y^3$, then we obtain the trajectory equation by solving Eq. (15): $\xi_p = k_L \mathcal{M} \lambda^2 \tau^2 / 2$ or, equivalently, $y = k_L \mathcal{M} R_y x^2 / (2L_{\text{Diff}}^2)$, which is a parabola, and is shown in Fig. 3(a) with green dashed line. We see that the theoretical result of the trajectory fits the numerical result well. The trajectory of SPs can be manipulated by changing the gradient k_L .

Figure 3(b) shows the dynamic deflect effect of the SPs soliton with a time-dependent external magnetic field $B_0(y, t) = k_T f(t) y$ with gradient $k_T = -0.3 \text{ T m}^{-1}$, $f(t) = \cos(3t/\tau_0)$. Corresponding equivalent potential $U_p = -k_T \mathcal{M} \xi_p \cos(3\tau)$, thus the trajectory equation is $\xi_p = k_T \mathcal{M} \lambda^2 [1 - \cos(3\tau)] / 9$ or, equivalently, $y = k_T \mathcal{M} \lambda^2 [1 - \cos(3x/\lambda L_{\text{Diff}})] / 9$ and it is a cosine curve. The green dashed line in Fig. 3(b) is given by the above analytic expression of the trajectory. We see that under a cosine-varied gradient magnetic field the trace of the SPs soliton is a cosine curve, and the numerical result agrees with the theoretical result well.

The technique of manipulating the SPs with gradient magnetic field, both of static and dynamic manipulating, may be useful for optical information processing.

V. XNOR-LIKE LOGIC GATE BASED ON DEFLECT EFFECT OF THE SP SOLITON

Based on the deflect effect of the SPs soliton, we designed a XNOR-like logic gate. We apply a time-dependent gradient magnetic field to the system. The gradient function has a triangle profile, which is given by $g(y) = ky \tanh(y/R_y)$, and the time variation is described by $f(t) = 2[h(\tau_1 - t/\tau_0) + h(t/\tau_0 - \tau_2)] - 1$, where $h(\tau)$ is the Heaviside unit step function, and τ_1 and τ_2 are the times at which the external gradient magnetic field changes its sign for the first time and the second time, respectively.

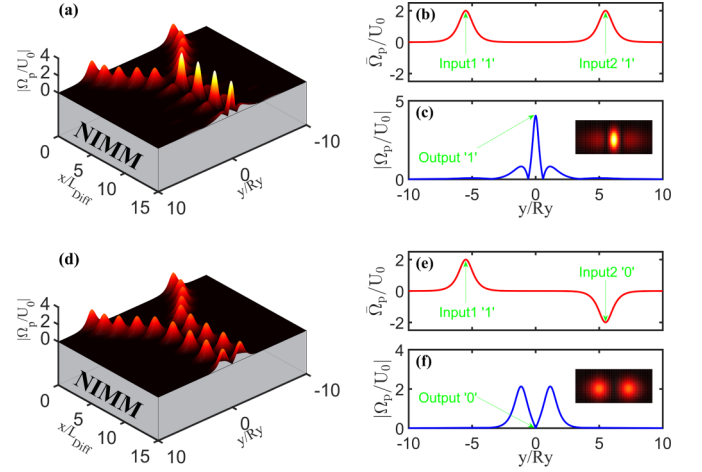


FIG. 4. Logical operation of the XNOR gate. (a) The 3D view of wave shape $|\Omega_p/U_0|$, (b) input signal amplitude $\bar{\Omega}_p/U_0 [\bar{\Omega}_p = \text{Re}(\Omega_p)]$, and (c) output signal wave shape $|\Omega_p/U_0|$ for the logical operation “1 XNOR 1=1.” (d) The 3D view of wave shape $|\Omega_p/U_0|$, (e) input signal amplitude $\bar{\Omega}_p/U_0 [\bar{\Omega}_p = \text{Re}(\Omega_p)]$, and (f) output signal wave shape $|\Omega_p/U_0|$ for the logical operation “1 XNOR 0=0.”

The input signals are two SPs solitons located in the symmetrical positions in the y axis with the same amplitude: $\Omega_p/U_0 = \eta \text{sech}[\eta(\xi + \xi_0)] \exp(\sigma_1 \pi i) + \eta \text{sech}[\eta(\xi - \xi_0)] \exp(\sigma_2 \pi i)$, where $\sigma_{1(2)} = 0, 1$ is the phase difference parameter, η is the amplitude parameter, and ξ_0 is the position parameter. If $|\sigma_1 - \sigma_2| = 1(0)$ then the phase difference of the two signals is $\pi(0)$. In our design, the value of $\sigma_{1(2)}$ is a “0 – 1” logical variable. In the following simulation, $k = -0.3 \text{ T m}^{-1}$, $\tau_1 = 0.8$, $\tau_2 = 1.4$, $\xi_0 = 5.5$, $\eta = -2$, and other parameters are the same as given above.

At the beginning, the two signals are distant from each other and the interaction between them is weak, and both of them will propagate straight to the other side of the NIMM waveguide. However, when the designed magnetic field is applied to the system, the gradient of the magnetic field is symmetrical about the x axis, thus the two input signals will deflect in the opposite direction, and they will grow closer to or more distant from each other, depending on the sign of the gradient of the magnetic field. In our system, they will grow closer to each other. As the distance between the two signals decreases, the interaction between them tends to be stronger, and they will be mutually attractive (the phase difference of the two input signals is zero) or mutually exclusive (the phase difference of the two input signals is π) [34]. The time variation is designed to change the sign of the magnetic gradient for two times, which will lead to the relative velocity (y component) of the two signals first accelerating from zero and then decreasing to near zero, and the relative distance decreases. When the sign of the magnetic gradient changes twice, the two SPs soliton signals will keep interacting and colliding periodically, and there will be an output signal in the other side of the NIMM waveguide.

As shown in Figs. 4(a) and 4(d), the two input signals come into the waveguide at position $x = 0$ and output a signal at position $x = 15L_{\text{Diff}}$. Figure 4(a) illustrates the case $|\sigma_1 - \sigma_2| = 0$, we set $\sigma_1 = \sigma_2 = 1$, and the input signal’s wave shape

$\bar{\Omega}_p/U_0[\bar{\Omega}_p = \text{Re}(\Omega_p)]$ is presented in Fig. 4(b). The same phase of the two SPs solitons causes attractive interaction, and the amplitude is enhanced when the two solitons collide. The enhanced center amplitude $|\Omega_p/U_0|$ is used as an output signal representing the logical “1,” demonstrated in Fig. 4(c). Thus, logical operation “1 XNOR 1=1” is realized. If the input is $\sigma_1 = \sigma_2 = 0$, the output will not change, and logical operation “0 XNOR 0=1” is obtained.

Figure 4(d) illustrates the wave shape $|\Omega_p/U_0|$ in the case $|\sigma_1 - \sigma_2| = 1$. We set $\sigma_1 = 1, \sigma_2 = 0$, and the input signal's wave shape $\bar{\Omega}_p/U_0[\bar{\Omega}_p = \text{Re}(\Omega_p)]$ is presented in Fig. 4(e). The π phase difference of the two SPs solitons causes exclusive interaction, and the amplitude becomes extremely small at the collision center when the two SPs solitons collide. This means a weak intensity of $|\Omega_p/U_0|$ will present at the collision center, and it can be used as an output signal representing the logical “0,” as shown in Fig. 4(f). Then we realize the logical operation “1 XNOR 0=0,” and if the input is $\sigma_1 = 0, \sigma_2 = 1$, we also can get the logical operation “0 XNOR 1=0.”

VI. CONCLUSIONS

In conclusion, we have proposed a scheme to manipulate SPs with external gradient magnetic field. We have shown that a lossless SPs soliton can be obtained in the NIMM-dielectric interface waveguide via ARG effect. And in this system, the

SPs soliton can be deflected in the external gradient magnetic field, both in a static and in a dynamic way, thus the trajectory of the SPs soliton can be manipulated by external gradient magnetic fields. Furthermore, we have designed a XNOR-like logic gate in a NIMM-ARG medium system with a special external gradient magnetic field. The results reported here suggest a way to manipulate SPs and may have potential applications for optical information processing.

ACKNOWLEDGMENTS

This work was supported by National Natural Science Foundation of China under Grants No. 11604185 and No. 11804196 and by China Postdoctoral Science Foundation under Grant No. 2017M612323.

Q.L. and N.L. contributed equally to this work.

APPENDIX A: THE TM MODE OF THE EM FIELD

The permittivity (ε_{r1}) and the permeability (μ_{r1}) of a NIMM can be described by the Drude model, i.e., $\varepsilon_{r1}(\omega_p) = \varepsilon_\infty - \omega_e^2/\omega_p(\omega_p + i\gamma_e)$, $\mu_{r1}(\omega_p) = \mu_\infty - \omega_m^2/\omega_p(\omega_p + i\gamma_m)$, where $\omega_{e,m}$ are electric and magnetic plasma frequencies of the NIMM, $\gamma_{e,m}$ are corresponding decay rates, and ε_∞ and μ_∞ are background constants.

The quantized probe field reads [3]

$$\mathbf{E}_p(\mathbf{r}, t) = \begin{cases} -\frac{c}{\omega_p \varepsilon_{r1}} (\beta \hat{\mathbf{z}} + ik_1 \hat{\mathbf{x}}) e^{k_1 z} e^{i(\beta x - \omega_p t)} \hat{E}_0 + \text{c.c.}, & z < 0 \\ -\frac{c}{\omega_p \varepsilon_{r2}} (\beta \hat{\mathbf{z}} - ik_2 \hat{\mathbf{x}}) e^{-k_2 z} e^{i(\beta x - \omega_p t)} \hat{E}_0 + \text{c.c.}, & z > 0 \end{cases} \quad (\text{A1})$$

where $k_j^2 = \beta^2 - \varepsilon_{rj} \mu_{rj} \omega_p^2 / c^2$ ($j = 1$ for the NIMM, $j = 2$ for the dielectric) satisfies the relation $k_1 \varepsilon_{r2} = -k_2 \varepsilon_{r1}$, which gives the propagation constant of the SPs, i.e., $\beta(\omega_p) = \omega_p [\varepsilon_{r1} \varepsilon_{r2} (\varepsilon_{r1} \mu_{r2} - \varepsilon_{r2} \mu_{r1}) / (\varepsilon_{r1}^2 - \varepsilon_{r2}^2)]^{1/2} / c$; $\hat{E}_0 = \sqrt{\hbar \omega_p / \varepsilon_0 V} \hat{a}(\omega_p)$ is the field operator; $\hat{a}(\omega_p)$ is the creation operator of TM photons; $V = L_x L_y L_z$ is the effective volume, where L_x and L_y are the lengths of the NIMM-dielectric interface in the x and y directions, respectively; and L_z is the effective length characterizing EM-field confinement in the z direction, which is defined as

$$L_z \equiv \sum_{j=1,2} \frac{1}{2 \text{Re}(k_j)} \left(\frac{\tilde{\varepsilon}_{rj} |\beta|^2 + |k_j|^2}{|\varepsilon_{rj}|^2 k_0^2} + \tilde{\mu}_{rj} \right), \quad (\text{A2})$$

with $\tilde{\varepsilon}_r \equiv \text{Re}[\partial(\omega_p \varepsilon_r) / \partial \omega_p]$, $\tilde{\mu}_r \equiv \text{Re}[\partial(\omega_p \mu_r) / \partial \omega_p]$.

When the dielectric is chosen as the ARG medium, and the photon number of the laser field is much larger than unity, thus $\hat{a}(\omega_p)$ can be taken as quantity function $a(\mathbf{r}, t)$; the pulsed EM field in the ARG medium then becomes $\mathbf{E}_p(\mathbf{r}, t) = \mathcal{E}_p(\mathbf{r}, t) \mathbf{u}_p(z) \exp[i(\beta x - \omega_p t)] + \text{c.c.}$, with $\mathcal{E}_p(\mathbf{r}, t) = \sqrt{\hbar \omega_p / \varepsilon_0 V} a(\mathbf{r}, t)$; and, according to Eq. (A1), the mode function reads $\mathbf{u}_p(z) = -c[\beta(\omega_p) \hat{\mathbf{z}} - ik_2(\omega_p) \hat{\mathbf{x}}] e^{k_2 z} / \varepsilon_{r2} \omega_p$.

In our analysis, the above system parameters are given by $\varepsilon_\infty = 1$, $\mu_\infty = 1$, $\omega_e = 1.37 \times 10^{16} \text{ s}^{-1}$, $\omega_m = 2.45 \times 10^{15} \text{ s}^{-1}$, $\gamma_e = 2.73 \times 10^{13} \text{ s}^{-1}$ (as for Ag), and $\gamma_m = \gamma_e / 1000$.

APPENDIX B: MULTISCALE METHOD AND THE EXPLICIT EXPRESSIONS OF THE FIRST- AND SECOND-ORDER SOLUTIONS

In multiscale method, the expansions of the derivative read $\partial/\partial t = \partial/\partial t_0 + \epsilon \partial/\partial t_1 + \epsilon^2 \partial/\partial t_2$, $\partial/\partial x = \partial/\partial x_0 + \epsilon \partial/\partial x_1 + \epsilon^2 \partial/\partial x_2$, $\partial/\partial y = \epsilon \partial/\partial y_1$. Substituting all expansions into the system equations, we obtain a series of linear but inhomogeneous equations in each order:

$$\left(i \frac{\partial}{\partial t_0} + d_2^{(0)} \right) A_2^{(j)} + A_3^{(0)*} \zeta_p^*(z) e^{-i\theta_p^*} \Omega_p^{*(j)} = M^{(j)}, \quad (\text{B1a})$$

$$\left(i \frac{\partial}{\partial t_0} + d_3^{(0)} \right) A_3^{(j)} + \Omega_c A_1^{(j)} = N^{(j)}, \quad (\text{B1b})$$

$$(A_1^{*(0)} A_1^{(j)} + A_3^{*(0)} A_3^{(j)}) + \text{c.c.} = P^{(j)}, \quad (\text{B1c})$$

$$\hat{L}_1 \Omega_p^{(j)} \zeta_p(z) e^{i\theta_p} + \kappa_{23} A_3^{(0)} A_2^{*(j)} = Q^{(j)}, \quad (\text{B1d})$$

and the expressions on the right-hand side of the above equations are

$$\begin{aligned}
 M^{(j)} = & h(j-2)(-1)\zeta_p^*(z)e^{-i\theta_p} \sum_{m=1}^{j-1} \Omega_p^{(j-m)} A_3^{(m)} \\
 & + h(j-2)(-1) \left(i \frac{\partial}{\partial t_1} + d_2^{(1)} \right) A_2^{(j-1)} \\
 & + h(j-3)(-1) \left(i \frac{\partial}{\partial t_2} + d_2^{(2)} \right) A_2^{(j-2)}, \quad (\text{B2})
 \end{aligned}$$

$$\begin{aligned}
 N^{(j)} = & h(j-2)(-1)\zeta_p(z)e^{i\theta_p} \sum_{m=1}^{j-1} \Omega_p^{(j-m)} A_2^{(m)} \\
 & + h(j-2)(-1) \left(i \frac{\partial}{\partial t_1} + d_3^{(1)} \right) A_3^{(j-1)} \\
 & + h(j-3)(-1) \left(i \frac{\partial}{\partial t_2} + d_3^{(2)} \right) A_3^{(j-2)} \\
 & + \delta_{1j}(-1)d_3^{(1)}A_3^{(0)} + \delta_{2j}(-1)d_3^{(2)}A_3^{(0)}, \quad (\text{B3})
 \end{aligned}$$

$$P^{(j)} = 2\delta_{0j} - h(j-2) \sum_{k=1}^3 \sum_{m=1}^{j-1} A_k^{j-m} A_k^{*(m)}, \quad (\text{B4})$$

$$\begin{aligned}
 Q^{(j)} = & h(j-2)(-1)i \left(\frac{\partial}{\partial x_1} + \frac{1}{n_{\text{eff}}} \frac{1}{c} \frac{\partial}{\partial t_1} \right) \Omega_p^{(j-1)} \zeta_p(z) e^{i\theta_p} \\
 & + h(j-3)(-1)i \left(\frac{\partial}{\partial x_2} + \frac{1}{n_{\text{eff}}} \frac{1}{c} \frac{\partial}{\partial t_2} \right) \Omega_p^{(j-2)} \zeta_p(z) e^{i\theta_p} \\
 & + h(j-3)(-1) \frac{1}{2\beta} \frac{\partial^2}{\partial y_1^2} \Omega_p^{(j-2)} \zeta_p(z) e^{i\theta_p} \\
 & + h(j-2)(-1)\kappa_{23} \sum_{m=1}^{j-1} A_3^{(j-m)} A_2^{*(m)}, \quad (\text{B5})
 \end{aligned}$$

where $h(x)$ is the Heaviside unit step function, and δ_{ij} is the Kronecker delta symbol. Note that in our analysis the external magnetic field is assumed to be the order of ϵ^2 , then in the above equations $d_{2(3)}^{(0)} = \Delta_{2(3)} + i\gamma_{2(3)}$, $d_{2(3)}^{(1)} = 0$, $\epsilon^2 d_{2(3)}^{(2)} = -\mu_{2(3)1} B(y)$. Solving the above equations order by order, we can obtain the solution in each order.

We define some new operators: $\hat{L}_1 = i(\partial/\partial x_0 + c^{-1}n_{\text{eff}}^{-1}\partial/\partial t_0)$, $\hat{L}_2 = i\partial/\partial t_0 + d_2^{(0)}$, $\hat{L} = \hat{L}_2^* \hat{L}_1 - \kappa_{23}|A_3^{(0)}|^2$, where \hat{L}_2^* is the conjugate operator of \hat{L}_2 . Then we obtain the formal solution of Eqs. (B1):

$$A_2^{(j)} = \frac{1}{\kappa_{23}A_3^{*(0)}} [Q^{*(j)} - \hat{L}_1^* \Omega_p^{*(j)} \zeta_p^*(z) e^{-i\theta_p^*}], \quad (\text{B6})$$

$$A_3^{(j)} = \frac{1}{d_3^{(0)}} (N^{(j)} - \Omega_c A_1^{(j)}), \quad (\text{B7})$$

and $\Omega_p^{(j)}$ satisfy $\hat{L} \Omega_p^{(j)} \zeta_p(z) e^{i\theta_p} = S^{(j)}$ with $S^{(j)} = \hat{L}_2^* Q^{(j)} - \kappa_{23} A_3^{(0)} M^{*(j)}$.

Then we will give the explicit form of the solutions in the first and second order.

1. First-order solutions

For the case $j = 1$, we can obtain $M^{(1)} = N^{(1)} = P^{(1)} = Q^{(1)} = S^{(1)} = 0$; then it reduces to linear problem $\hat{L} \Omega_p^{(1)} = 0$. So we introduce a trial solution $\Omega_p^{(1)} = \mathcal{F} \exp(i\theta)$, where \mathcal{F} is the slowly varying envelope of the probe field (a function of slow variables), $\theta = K(\omega)x_0 - \omega t_0$. From the formal solution, we obtain

$$A_1^{(1)} = A_3^{(1)} = 0, \quad (\text{B8})$$

$$\begin{aligned}
 A_2^{(1)} &= \frac{A_3^{(0)}}{\omega - d_2^{(0)}} \mathcal{F}^* e^{-i\theta^*} \zeta_p^*(z) e^{-i\theta_p^*} \\
 &= a_2^{(1)} \mathcal{F}^* e^{-i\theta^*} \zeta_p^*(z) e^{-i\theta_p^*}. \quad (\text{B9})
 \end{aligned}$$

2. Second-order solutions

For the case $j = 2$, we can obtain the expressions of $M^{(2)}$, $N^{(2)}$, $P^{(2)}$, $Q^{(2)}$, $S^{(2)}$ by substituting the zeroth- and first-order solutions into Eqs. (B2)–(B5). The eigenproblem of $\Omega_p^{(2)}$ gives $\Omega_p^{(2)} = 0$, then we obtain the second-order solution:

$$A_1^{(2)} = a_{11}^{(2)} |\mathcal{F}|^2 e^{-2\theta''} |\zeta_p(z)|^2 e^{-2\theta_p''} + a_{12}^{(2)}, \quad (\text{B10})$$

$$A_2^{(2)} = a_2^{(2)} \frac{\partial \mathcal{F}^*}{\partial t_1} e^{-i\theta^*} \zeta_p^*(z) e^{-i\theta_p^*}, \quad (\text{B11})$$

$$A_3^{(2)} = a_{31}^{(2)} |\mathcal{F}|^2 e^{-2\theta''} |\zeta_p(z)|^2 e^{-2\theta_p''} + a_{32}^{(2)}, \quad (\text{B12})$$

with the coefficients

$$\begin{aligned}
 a_{11}^{(2)} &= \frac{1}{2A_1^{(0)}} \frac{|A_3^{(0)}|^2}{|\Omega_c|^2 + |d_3^{(0)}|^2} \\
 &\quad \times \frac{d_3^{(0)}(\omega - d_2^{(0)}) + \text{c.c.} - |d_3^{(0)}|^2}{|\omega - d_2^{(0)}|^2}, \quad (\text{B13a})
 \end{aligned}$$

$$a_{12}^{(2)} = \frac{1}{2A_1^{(0)}} \frac{|A_3^{(0)}|^2}{|\Omega_c|^2 + |d_3^{(0)}|^2} (d_3^{(2)} d_3^{*(0)} + \text{c.c.}), \quad (\text{B13b})$$

$$a_2^{(2)} = \frac{i}{\kappa_{23} A_3^{*(0)}} \left(\frac{1}{n_{\text{eff}}} \frac{1}{c} - \frac{1}{V_g^*} \right), \quad (\text{B13c})$$

$$a_{31}^{(2)} = -\frac{a_{11}^{(2)} \Omega_c}{d_3^{(0)}} - \frac{A_3^{(0)}}{d_3^{(0)}(\omega - d_2^{(0)})}, \quad (\text{B13d})$$

$$a_{32}^{(2)} = -\frac{a_{12}^{(2)} \Omega_c}{d_3^{(0)}} - \frac{d_3^{(2)}}{d_3^{(0)}} A_3^{(0)}, \quad (\text{B13e})$$

where $\theta'' = \text{Im}(\theta)$, $\theta_p'' = \text{Im}(\theta_p)$.

[1] K. MacDonald and N. Zheludev, *Laser Photonics Rev.* **4**, 562 (2010).

[2] M. S. Tame, K. R. McEnery, S. K. Özdemir, J. Lee, S. A. Maier, and M. S. Kim, *Nat. Phys.* **9**, 329 (2013).

- [3] A. Kamli, S. A. Moiseev, and B. C. Sanders, *Phys. Rev. Lett.* **101**, 263601 (2008).
- [4] S. A. Moiseev, A. A. Kamli, and B. C. Sanders, *Phys. Rev. A* **81**, 033839 (2010).
- [5] M. Siomau, A. A. Kamli, S. A. Moiseev, and B. C. Sanders, *Phys. Rev. A* **85**, 050303(R) (2012).
- [6] B. R. Lavoie, P. M. Leung, and B. C. Sanders, *Phys. Rev. A* **88**, 023860 (2013).
- [7] S. Asgarneshad-Zorgabad, R. Sadighi-Bonabi, and B. C. Sanders, *Phys. Rev. A* **98**, 013825 (2018).
- [8] S. Asgarneshad-Zorgabad, P. Berini, and B. C. Sanders, *Phys. Rev. A* **99**, 051802(R) (2019).
- [9] N. Khan, B. Amin Bacha, A. Iqbal, A. Ur Rahman, and A. Afaq, *Phys. Rev. A* **96**, 013848 (2017).
- [10] C. Tan and G. Huang, *Phys. Rev. A* **89**, 033860 (2014).
- [11] C. Tan and G. Huang, *Phys. Rev. A* **91**, 023803 (2015).
- [12] L. Li, T. Li, S. Wang, S. Zhu, and X. Zhang, *Nano Lett.* **11**, 4357 (2011).
- [13] Y. Fu, X. Hu, C. Lu, S. Yue, H. Yang, and Q. Gong, *Nano Lett.* **12**, 5784 (2012).
- [14] A. V. Krasavin and N. I. Zheludev, *Appl. Phys. Lett.* **84**, 1416 (2004).
- [15] A. V. Zayats and S. Maier, *Active Plasmonics and Tuneable Plasmonic Metamaterials* (Wiley, New York, 2013), Vol. 8.
- [16] N. Jiang, X. Zhuo, and J. Wang, *Chem. Rev.* **118**, 3054 (2018).
- [17] G. A. Wurtz, W. Hendren, R. Pollard, R. Atkinson, L. L. Guyader, A. Kirilyuk, T. Rasing, I. I. Smolyaninov, and A. V. Zayats, *New J. Phys.* **10**, 105012 (2008).
- [18] V. I. Belotelov, L. E. Kreilkamp, I. A. Akimov, A. N. Kalish, D. A. Bykov, S. Kasture, V. J. Yallapragada, A. Venu Gopal, A. M. Grishin, S. I. Khartsev, M. Nur-E-Alam, M. Vasiliev, L. L. Doskolovich, D. R. Yakovlev, K. Alameh, A. K. Zvezdin, and M. Bayer, *Nat. Commun.* **4**, 2128 (2013).
- [19] C. Clavero, K. Yang, J. R. Skuza, and R. A. Lukaszew, *Opt. Express* **18**, 7743 (2010).
- [20] K. F. MacDonald, Z. L. Sámson, M. I. Stockman, and N. I. Zheludev, *Nat. Photonics* **3**, 55 (2008).
- [21] L. Karpa and M. Weitz, *Nat. Phys.* **2**, 332 (2006).
- [22] D. L. Zhou, L. Zhou, R. Q. Wang, S. Yi, and C. P. Sun, *Phys. Rev. A* **76**, 055801 (2007).
- [23] A. Karnieli and A. Arie, *Phys. Rev. Lett.* **120**, 053901 (2018).
- [24] A. Karnieli and A. Arie, *Optica* **5**, 1297 (2018).
- [25] Z. Chen and G. Huang, *Phys. Rev. A* **89**, 033817 (2014).
- [26] G. Huang, L. Deng, and M. G. Payne, *Phys. Rev. E* **72**, 016617 (2005).
- [27] R. Thomas, C. Kupchak, G. S. Agarwal, and A. I. Lvovsky, *Opt. Express* **21**, 6880 (2013).
- [28] D. A. Steck, Rubidium 85 D Line Data, <http://steck.us/alkalidata>.
- [29] L. J. Wang, A. Kuzmich, and A. Dogariu, *Nature (London)* **406**, 277 (2000).
- [30] G. M. Gehring, A. Schweinsberg, C. Barsi, N. Kostinski, and R. W. Boyd, *Science* **312**, 895 (2006).
- [31] H. J. Li, C. Hang, G. Huang, and L. Deng, *Phys. Rev. A* **78**, 023822 (2008).
- [32] A. B. Aceves, J. V. Moloney, and A. C. Newell, *Phys. Rev. A* **39**, 1809 (1989).
- [33] E.-H. Majid, K. M.-F. Mohammad, and Z. Abbas, *Appl. Opt.* **48**, 5005 (2009).
- [34] Y. S. Kivshar and G. Agrawal, *Optical Solitons: From Fibers to Photonic Crystals* (Academic, New York, 2003).